18th AIAA/CEAS Aeroacoustics Conference (33rd AIAA Aeroacoustics Conference)
04 - 06 June 2012, Colorado Springs, CO

AIAA 2012-2081

Full-Scale Jet Noise Characterization Using Scan-Based Acoustical Holography*, †

Alan T. Wall,[1] Kent L. Gee,[2] Tracianne B. Neilsen,[3] and David W. Krueger,[4]
Brigham Young University, Provo, UT 84602, USA

Michael M. James[5]
Blue Ridge Research and Consulting, Asheville, NC 28801, USA

and

Scott D. Sommerfeldt[6] and Jonathan D. Blotter[7]
Brigham Young University, Provo, UT 84602, USA

Array-based visualization techniques have been used for several decades to explore jet-noise properties such as source strength, size, and distribution. However, near-field acoustical holography (NAH) has only recently been utilized to study jet noise, and experiments are typically performed on laboratory jets in controlled environments. In this work, NAH was applied to measurements of a full-scale, installed jet engine. This paper outlines three different NAH methods applied to the data and addresses practical problems faced when NAH is performed on a full-scale jet. Holographic reconstruction of the jet-noise field at low frequencies shows phenomena consistent with radiation from large-scale turbulence structures. A comparison of reconstructed levels using both planar and cylindrical NAH methods suggests that cylindrical NAH outperforms planar NAH for jet noise sources.

I. Introduction

NEAR-FIELD acoustical holography (NAH) is a useful tool for characterizing both the near sound field and the sources of jet noise.[1-4] In any of the various forms of NAH, the measured sound field, or "hologram," is represented as a superposition of wavefunctions radiated from simple sources, be they planar, cylindrical, or

* SBIR DATA RIGHTS - (DFARS 252.227-7018 (JUNE 1995)); Contract Number: FA8650-08-C-6843;
Contractor Name & Address: Blue Ridge Research and Consulting, LLC, 15 W Walnut St., Suite C; Asheville, NC
Expiration of SBIR Data Rights Period: March 17, 2016 (Subject to SBA SBIR Directive of September 24, 2002)
The Government's rights to use, modify, reproduce, release, perform, display, or disclose technical data or computer software marked with this legend are restricted during the period shown as provided in paragraph (b)(4) of the Rights in Noncommercial Technical Data and Computer Software—Small Business Innovation Research (SBIR) Program clause contained in the above identified contract. No restrictions apply after the expiration date shown above. Any reproduction of technical data, computer software, or portions thereof marked with this legend must also reproduce the markings.
† Distribution A – Approved for Public Release; Distribution is Unlimited 88ABW-2012-2279.
[1] Corresponding Author, Department of Physics and Astronomy, N283 ESC Provo, UT 84602, Student Member.
[2] Associate Professor, Department of Physics and Astronomy, N283 ESC, Provo, UT 84602, AIAA Senior Member.
[3] Part-time Professor, Department of Physics and Astronomy, N283 ESC, Provo, UT 84602.
[4] Student, Department of Physics and Astronomy, N283 ESC, Provo, UT 84602.
[5] Vice President and Senior Principal Engineer, Blue Ridge Research and Consulting, 15 W. Walnut St. Suite C, Asheville, NC 28801.
[6] Dean and Professor, College of Physical and Mathematical Sciences, N181B ESC, Provo, UT 84602.
[7] Professor, Department of Mechanical Engineering, 435Q CTB, Provo, UT 84602.

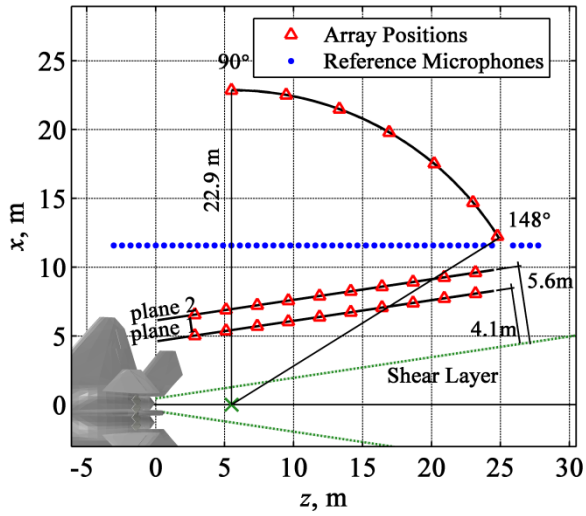

Figure 1 Schematic of the measurement locations relative to the aircraft. Projections onto the *x*-*z* plane of the surface measurements plane 1, plane 2, and the arc are designated by black lines. The arc has a radius of 22.9 m, and it is centered on the estimated source region (marked by a green "x"). The locations of the field array, the composite of which make up the measurement surfaces, are marked by red triangles. In this paper, plane 2 was used as the hologram measurement for planar implementations of NAH. The linear ground-based microphone array at 11.7 m from the jet centerline, marked by blue dots, served both as a reference signal array for the planar measurement and as a hologram measurement for cylindrical NAH.

spherical waves.[5] Knowledge of these wavefunctions in one location allows for the extrapolation of the sound field to any other location in a source-free medium. Thus, each wavefunction is individually propagated to a desired reconstruction location, and the superposition of these waves provides an estimate of the total reconstructed sound field at that location. NAH provides any acoustic quantity–pressure, particle velocity, or intensity–in a three-dimensional region near a two-dimensional holographic measurement. It has been used to explore the near sound field and to produce equivalent source models of high-power jet noise.[4,6,7]

It is commonly accepted that jet noise sources consist of two distinct components: large-scale turbulent structures and small-scale turbulence.[8,9] The radiation from the large-scale structures dominates the sound field, particularly in the aft direction. This radiation is directional and can be compared to Mach-wave radiation, or radiation from a wavy-wall-like structure that is convecting downstream with supersonic velocity components. Characteristic frequencies radiated by large-scale structures tend to be lower in frequency than the characteristic frequencies of the small-scale turbulence.[10] Phenomena of high-power jet-noise radiation at low frequencies, which are consistent with established properties of large-scale turbulence structures, are the focus of this paper.

NAH measurements were made on the jet produced by a single engine of the F-22A Raptor. A scan-based two-dimensional hologram in the geometric near field of the jet was measured using a small, dense, mobile array of microphones. A second, one-dimensional, ground-based array of microphones was also used. This paper presents the methodology and sound-field reconstructions obtained from the implementation of three different NAH methods on the jet. Data from both microphone arrays are used in the various NAH methods.

This paper is organized as follows. Section II provides a summary of the NAH experiment performed on the jet. A detailed outline of the methodology implemented in the sound-field reconstruction process is given in Section III. This includes a description of, and solutions for, the problems encountered in applying NAH to a full-scale jet. Section IV contains reconstruction results obtained from the three NAH methods. The effectiveness of each method in the jet-noise field is compared, and phenomena of large-scale turbulent structures are identified. Conclusions are given in Section V.

II. Experiment Summary

Although only a brief review of measurement procedures is given here, comprehensive descriptions may be found in Refs. 11 and 12. The aircraft used was a Lockheed Martin/Boeing F-22A Raptor, a fifth-generation military

fighter jet designed for air dominance and precision ground attack. The Raptor has two Pratt & Whitney F119-PW-100 turbofan engines that are each in the 160 kN (35,000 lbf) thrust class. The engines have two-dimensional convergent-divergent nozzles capable of ±20° thrust vectoring. All measurements were made with the aircraft tied down to a run-up pad, while the engine closest to the measurement arrays (see Fig. 1) was cycled through four power conditions: idle, intermediate, military, and full afterburner, while the other engine was held at idle.

The field array used in this experiment allowed for a series of dense, large-aperture, two-dimensional measurements of the sound field.[11] It was comprised of 90 6.35-mm (0.25-in) GRAS 40BE prepolarized microphones, arranged in 5 rows and 18 columns with 0.15-m (6.0-in) equal spacing. The field array was mounted to an extruded aluminum guide rail to allow for easy and precise placement. It measured the geometric near field of the jet in a series of "scans." The *x*-*z* locations of the field-array scans are designated by red triangles in Fig. 1. (The *y*-axis is in the vertical direction, measured from the ground up.) Subsets of scans were patched together in both the horizontal and vertical directions to make the two-dimensional measurement planes 1 and 2, which are marked by black lines. In addition, an arc-shaped surface was measured in the transition region from the near to the far field. The arc was centered at a point 5.5 m downstream of the nozzle (marked by a green "x"), and had a radius of 22.9 m. The angles shown are referenced to the front of the aircraft.

A second array of 50 microphones, called the reference array, was placed along the ground 11.7 m from the jet centerline with 0.61 m spacing. The location of this array was fixed throughout the measurement, and these microphones recorded sound pressures simultaneously with the roving field array. Their locations are marked by blue dots in Fig. 1. The reference array served two purposes: (1) to allow for the generation of coherent field measurements from temporally distinct scans,[4,13] and (2) as an additional, simultaneous hologram measurement for the implementation of cylindrical NAH. Several variants of GRAS Type I microphones, ranging from 3.18 mm to 6.35 mm in diameter, were used in the reference array.

III. Holography Methods

Since the development of NAH by Williams and Maynard[14] in 1980, several augmentations and adaptations of NAH have emerged. These include, but are not limited to, NAH for sources of various geometries,[5,15] improved filtering in the inverse problem,[16] source reconstruction using a limited measurement aperture[17,18] or reconstruction of a limited portion of the source,[19,20] and measurement of multiple independent sources in a scan-based approach.[2,13,21] Many of these elements of NAH processing have been used in the subsequent analyses.

The purpose of this section is not to give a comprehensive overview of NAH methods. Rather, it is designed to illuminate key aspects of NAH methods that have been used to study jet noise in this experiment. Subsections IIIA and B address some important preprocessing techniques to prepare the measured data for holographic projection. Subsection IIIC covers the basics of the several NAH methods implemented on the data.

A. Partial Field Decomposition

The scan-based near-field measurement was performed using the field array discussed in Sec. II. Each scan provided a dense measurement over a small patch of the jet near field. The field array scanned multiple locations to afford a large measurement aperture. This resulted in a set of temporally distinct scans with no fixed magnitude and phase relationships, i.e., the individual scans were incoherent. However, NAH processing requires a coherent hologram. Therefore, multireference partial field decomposition (PFD) was employed to tie together the incoherent scans of plane 2.

With the use of the reference array, the PFD method called virtual coherence was implemented on the scan-based data,[13,22] resulting in a set of mutually incoherent partial fields. Each partial field is a self-coherent hologram, yet independent from all other partial fields. The partial fields calculated with the virtual coherence method are ordered according to their relative strengths. Thus, the first partial fields correspond to the most prominent noise sources. Theoretically, the first partial fields are coherent with radiated jet noise sources, and the remaining partial fields correspond to measurement noise. A method for determining the number of source-related fields is given in Refs. 1 and 13. Although a quantitative treatment of the number of partial fields related to jet-noise sources is not given in this paper, it is insightful to see the decomposed fields and compare their relative strengths. (Some quantitative analyses of the appropriate number of partial fields for this experiment are provided in Ref. 4.

Figure 2 shows the PFD of the hologram measurement at plane 2 and 105 Hz for the engine operating at military conditions. All data locations are projected onto the *y*-*z* plane. The measured sound pressure levels (SPLs) are shown in Fig. 2a, and the SPLs of the first four partial fields are shown in Fig. 2b. The color range of all plotted levels spans exactly 30 decibels to facilitate comparison. The first partial field contains much higher levels than the second,

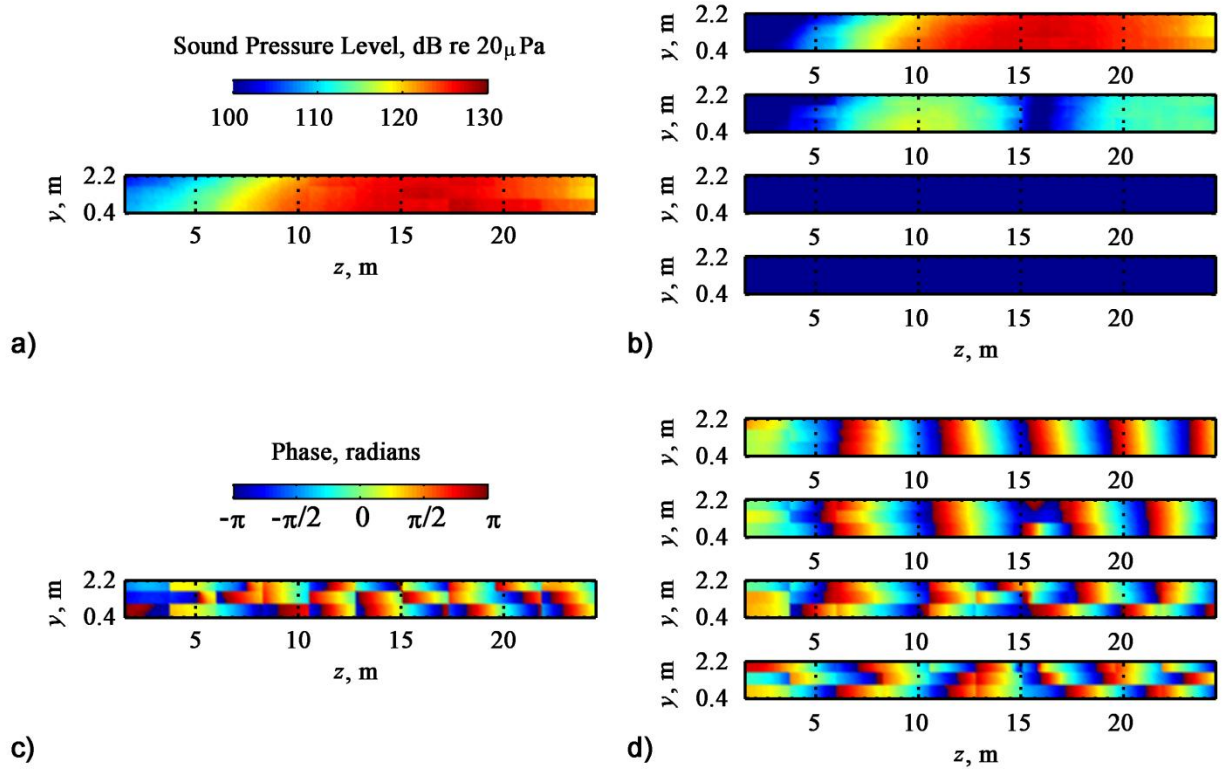

Figure 2. Virtual-coherence processing for measurements made at military engine conditions and for 105 Hz. All data locations are projected onto the *y*-*z* plane. a) The measured SPLs at plane 2. b) The SPLs of the first four partial fields. c) The discontinuous measured phase angles at plane 2. d) The phase angles of the first four partial fields.

and partial fields three and four have no levels less than 30 decibels below the maximum. Therefore, at 105 Hz and for military engine conditions, most of the sound field energy is contained within the first two partial fields.

To demonstrate the ability of PFD to generate coherent partial fields from an incoherent measurement, the phases corresponding to the magnitudes of the measured data are shown in Fig. 2c, and the phases of the first four partial fields are shown in Fig. 2d. Note the sharp phase discontinuities between the individual measured scans, which give Fig. 2c a "patchwork" appearance. By comparison, these discontinuities are smoothed out into fixed-phase relationships across most of the first two partial fields shown in Fig. 2d. The third and fourth partial fields still have a patchwork appearance, i.e. no fixed-phase relationship is found. This suggests that these low-amplitude regions of the partial fields are related to measurement noise, whereas the high-amplitude regions tend to be coherent with actual source radiation.

The ordering of partial fields according to relative strengths makes PFD a useful tool for providing qualitative information about the number of effective, independent subsources within an aeroacoustic source. For example, the two high-amplitude partial fields of Fig. 2 suggest that the radiation from the jet at military conditions and at 105 Hz can be represented by about two independent subsources.

The number of independent subsources in a jet depends on frequency. To show this, the PFD analysis performed at 105 Hz was repeated for 210 Hz, and is shown in Fig. 3. Again, the measured levels and phase values are plotted in Figs. 3a and c, respectively. The levels and phase values of the first four partial fields are plotted in Figs. 3b and d, respectively. Note that significant energy and structure are contained in all four partial fields shown in Fig. 3b. The physical locations of high-amplitude regions in Fig. 3b also correspond to regions of coherent phase relationships in Fig. 3d. This suggests the existence of four or more independent subsources at 210 Hz. In fact, although they are not all shown, the first seven partial fields contain levels within 30 decibels of the maximum level of the first partial field. Additional analysis of higher frequencies has indicated rapid increase in the number of independent subsources (or partial fields) required to represent the total measured sound field as frequency increases.[4]

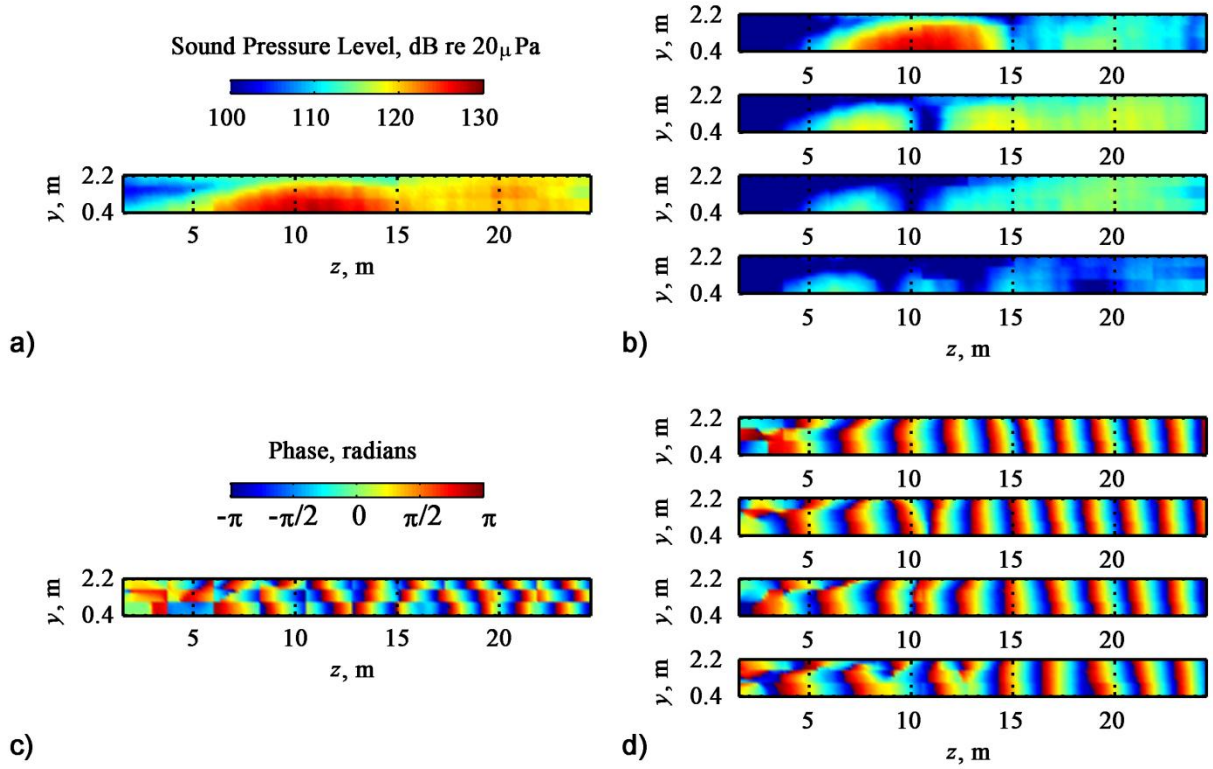

Figure 3. Virtual-coherence processing for measurements made at military engine conditions and for 210 Hz. All data locations are projected onto the *y*-*z* plane. a) The measured SPLs at plane 2. b) The SPLs of the first four partial fields. c) The discontinuous measured phase angles at plane 2. d) The phase angles of the first four partial fields.

B. Aperture Extension

When a hologram measurement aperture does not sufficiently span the source large errors can occur due to edge effects and wraparound.[23] Such is the case for the hologram measurements made in this experiment. To mitigate this problem, numerical procedures have been employed to extend the effective aperture of the data for each partial field. Thus, a sufficiently large aperture is provided, which approximates the sound field in the extended region and has pressure values that approach zero near the edges. The extension procedure is outlined in this subsection. The result of an example aperture extension is shown in Fig. 4. It is the extended hologram for the first partial field, from the 105 Hz measurement, with the engine at military conditions.

The first step in the aperture extension procedure is to "mirror" the data over the reflecting plane at the ground. This makes use of the fact that measurements were made over the concrete run-up pad, which can be considered a perfect reflector at frequencies of interest. The partial field data are outlined by the black rectangle in Fig. 4. The reflected data are outlined by the dashed rectangle. The method of images ensures that this is equivalent to a measurement of the jet source and an image source in free-field conditions.[24] After the data are mirrored, pressures in the spatial gap between the two surfaces are interpolated.

The next step is to perform numerical data-extrapolation. Several extrapolation procedures exist.[14,15] The accuracy of each method in approximating data outside the aperture depends on the nature of the measured data.[25] Analytic continuation has been shown to be a stable method,[17] and it was used in this study. The analytically continued data for the partial field are shown Figure 4. Note that the SPLs transition smoothly from the values at the edge of the measured/mirrored aperture toward values near zero at the edge of the extrapolated aperture.

C. Implementations of NAH

Three NAH methods were applied to the jet noise measurement: traditional holography based on a planar, spatial discrete Fourier transform of the complex pressures in the hologram (planar DFT-based NAH); planar, statistically

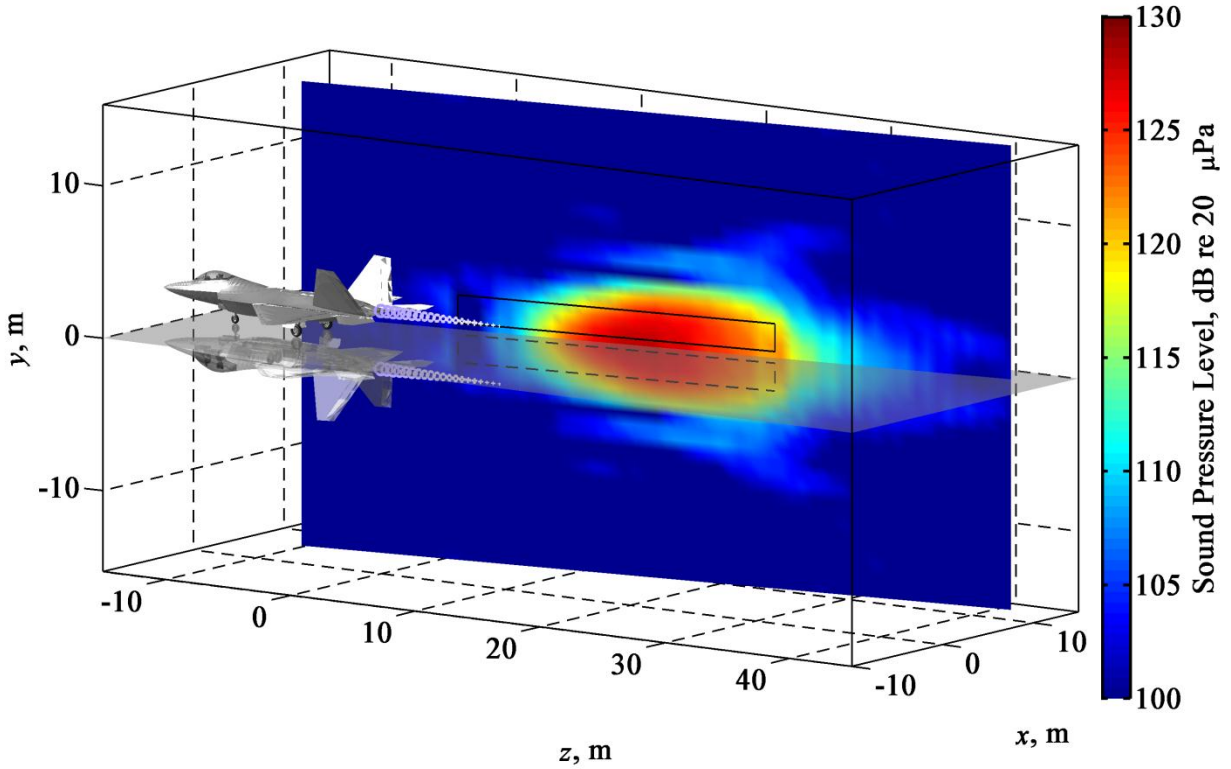

Figure 4. Illustration of the numerical data-extension method performed on each of the partial fields prior to NAH propagation. (The extended aperture of the first partial field, for the measurement at 105 Hz, with the engine operating at military conditions is shown here.) The measured data location is outlined by a solid black rectangle. (1) The data were "mirrored" over the reflecting plane at the ground. Mirrored data are outlined by the dashed rectangle. (2) Data between the measured and mirrored data were interpolated. (3) Analytic continuation was implemented to extend the resulting data to the full aperture shown here.

optimized near-field acoustical holography (SONAH); and cylindrical DFT-based NAH. The first two methods rely on a representation of the sound field as a superposition of plane waves, and both make use of the data resulting from the PFD and analytic continuation of pressures measured at plane 2. These two methods are the focus of this analysis. A brief mention is made in this paper of the third NAH method, which uses the data from the linear reference array as the hologram measurement, instead of the planar field measurements. It represents the sound field as a superposition of cylindrical waves instead of plane waves. These three methods are explained here, and sound-field reconstruction results from each are provided in Sec. IV.

Planar DFT-based NAH, developed by Williams and Maynard,[14,23] is the first and most straightforward NAH method used here. In this method, a planar DFT is applied in the two spatial dimensions of the hologram, which transforms the complex pressures from the spatial dimension into wavenumber space.[5] This means that every wavenumber component pair (i.e. each wavenumber has a component in two dimensions) corresponds to a unique plane wave; the superposition of the set of plane waves makes up the total measured sound field. Modified Tikhonov regularization is applied, in conjunction with the Morozov discrepancy principle, to filter out noise contained in evanescent-wavenumber components.[16] Without regularization, the propagation of this noise would cause the reconstructed sound field to blow up towards the source. A propagator is then applied, which generates the wavenumber-space representation of the sound field at another desired location. Finally, the inverse DFT is taken to give the reconstructed sound field at that location. DFT-based NAH is computationally simple, and fast.

Hologram requirements for DFT-based NAH include a coherent measurement, an evenly-spaced grid with spacing shorter than one half of the smallest acoustic wavelength of interest, and an aperture that spans beyond the region of the source and tapers toward zero at the edges. The measurement setup and the use of the aperture extension method described in Sec. IIIB ensured that these requirements were satisfied.

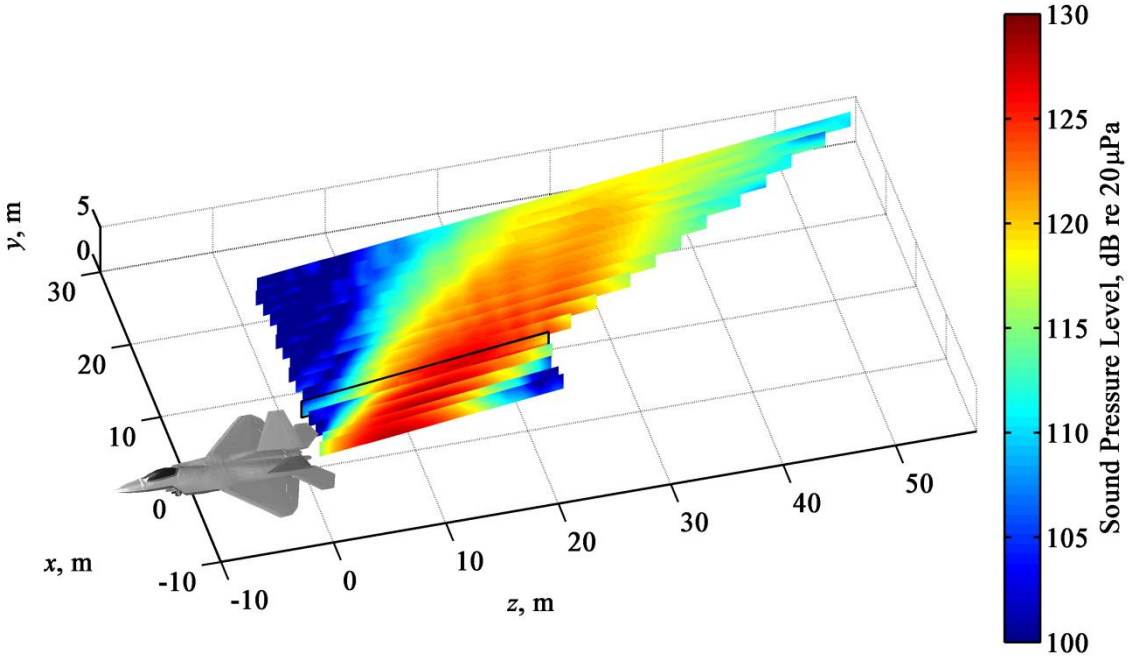

Figure 5. Sound pressure levels (SPLs) at 105 Hz (narrowband) reconstructed using planar DFT-based NAH. The engine was operating at military engine conditions. The original measurement is outlined in black.

The second method used was statistically-optimized near-field acoustical holography (SONAH).[20] SONAH is one of several patch NAH methods that avoid the requirement to measure an area much larger than the source, because they bypass the DFT procedure. The tradeoff for this advantage is a significantly longer computation time and larger memory requirements. In SONAH, the sound field at a desired location near the hologram measurement is calculated using a transfer matrix between the hologram and reconstruction locations. Although the aperture requirements for SONAH are not as stringent as the requirements for DFT-based NAH, it was found that some aperture extension was still required to produce optimal reconstruction results. Therefore, the PFD and the aperture extension methods described previously, as well as modified Tikhonov regularization, were implemented prior to SONAH propagation. The planar version of SONAH was used in this experiment.

A third NAH method is currently being investigated as a viable jet-noise visualization tool for this experiment: cylindrical NAH.[26] A representation of the sound field by cylindrical waves can be performed using both DFT-based NAH[5] and SONAH[27] methods. In this work the data measured by the reference microphones, which ran parallel to the jet centerline (see Fig. 1), served as the hologram measurement. Cylindrical DFT-based NAH was applied. Since these data were measured simultaneously, the hologram was coherent. Therefore, no PFD was required. However, a similar procedure, called spatial transformation of sound fields,[28,29] was used to allow for averaging and a smooth hologram. Then, a one-dimensional aperture extension using analytic continuation was implemented to ensure the data taper toward zero at the edges. As an approximation, azimuthal symmetry was assumed.[30] Although the azimuthal symmetry assumption is not a perfect representation of the geometrical locations of the jet source and its reflected image source, cylindrical NAH provides very promising reconstruction results.

IV. Holography Results

The three-dimensional sound fields reconstructed using the NAH methods described in Section III are presented in this section. All results shown in this paper are for the aircraft operating at military engine conditions, and most data shown are plotted on a color axis that spans 100 to 130 dB re 20 μPa. First, the planar DFT-based NAH results at 105 Hz are shown in Fig. 5. Average SPLs measured at plane 2 are outlined by the black rectangle. All other SPL values shown are reconstructed from these data after the implementation of planar DFT-based NAH. Most planes shown are perpendicularly spaced approximately 1.5 m apart. The reconstruction plane closest to the jet lies approximately along the boundary of the shear layer. Figure 5 clearly demonstrates the directionality of the jet noise

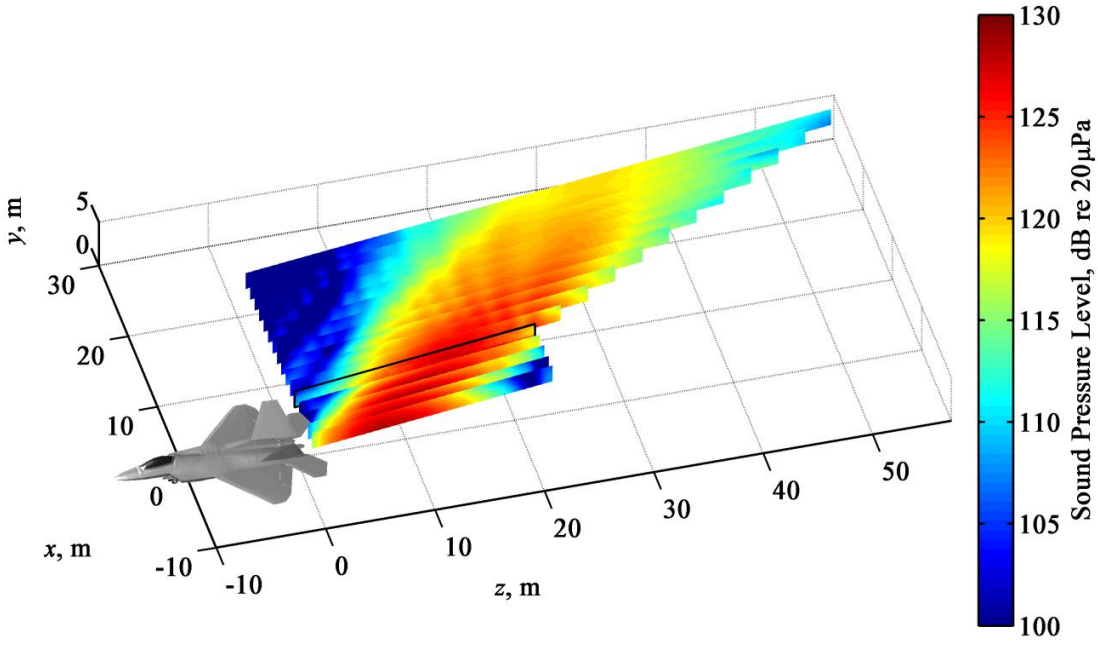

Figure 6. Sound pressure levels (SPLs) at 105 Hz (narrowband) reconstructed using planar SONAH. The engine was operating at military engine conditions. The original measurement is outlined in black.

source at 105 Hz. The highest levels occur in a single lobe that radiates at a large polar angle relative to the front of the aircraft.

Figure 6 shows the reconstructed SPLs obtained from the implementation of planar SONAH for the same frequency (105 Hz) and in the same locations as those shown in Fig. 5. At 105 Hz the reconstructed SPLs using SONAH are nearly identical to those obtained from a DFT-based NAH approach. Thus, provided that the general requirements for NAH are met (i.e. dense grid spacing and a sufficiently large aperture), then both of the NAH methods that represent the sound field as a superposition of plane waves (planar DFT-based NAH and planar SONAH) give similar reconstructions of jet noise.

To provide a quantitative comparison of the two reconstruction methods, SPLs reconstructed at the location of

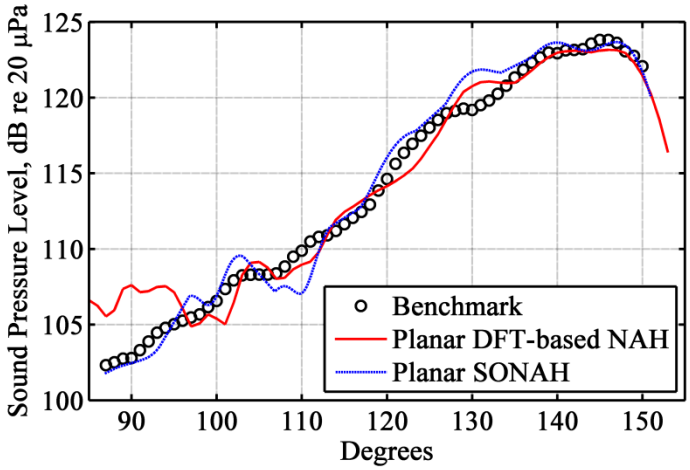

Figure 7. Reconstructed levels at 105 Hz, along the middle row of the arc (a height of y = 1.9 m), at a radial distance of 22.9 m, with polar angles measured relative to the front of the aircraft and the arc centered on a point 5.5 m downstream of the nozzle (see Fig.1). The results of both planar DFT-based NAH and planar SOANH are shown, along with a benchmark measurement.

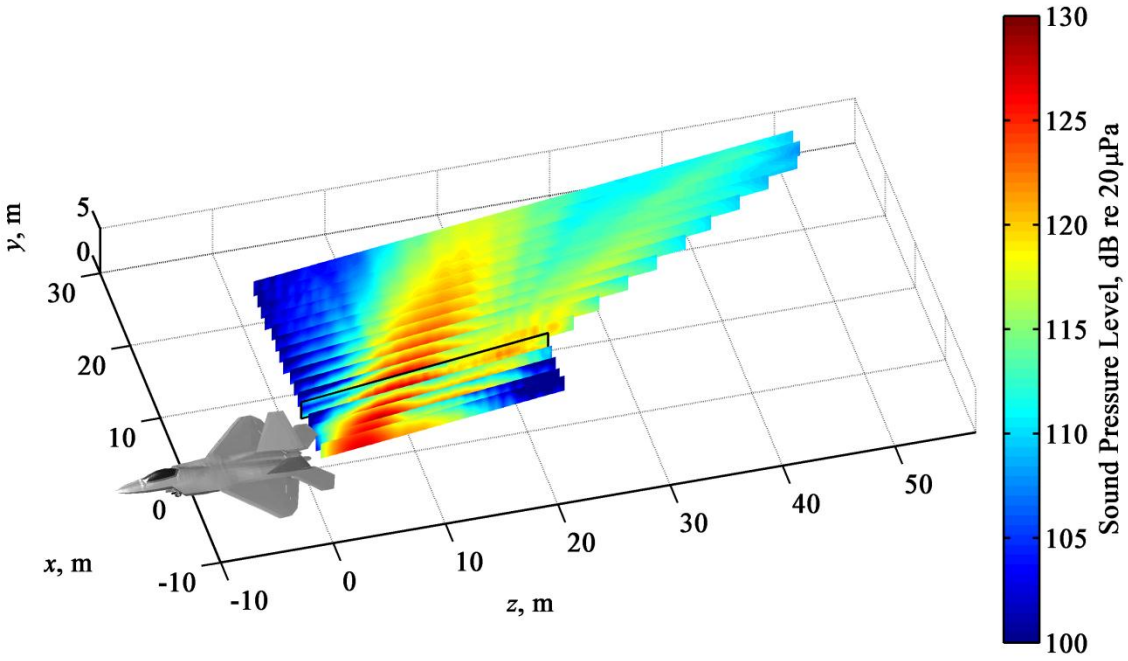

Figure 8. Sound pressure levels (SPLs) at 210 Hz (narrowband) reconstructed using planar DFT-based NAH. The engine was operating at military engine conditions. The original measurement is outlined in black.

the arc measurement using both planar DFT-based NAH and planar SONAH are shown in Fig. 7. The locations of these reconstructed levels are at y = 1.9 m (corresponding the height of the jet centerline), and at all angles along the arc. Both NAH methods in the high-amplitude region yield levels within 1-2 decibels from the benchmark. Any plane-wave representation of the jet noise field yields a similar reconstruction, regardless of the NAH method used.

The planar DFT-based NAH reconstruction at 210 Hz is shown in Fig. 8. If these levels are compared to the levels shown in Fig. 5, it can be seen that the sound field is significantly quieter at 210 Hz than at 105 Hz. This is consistent with the relative spectral levels shown in Ref. 12, Fig. 10. In addition, note how the main lobe at 210 Hz radiates in a direction that is farther forward than the lobe at 105 Hz. Thus, the directionality of the radiation from large-scale turbulence structures moves towards shallower polar angles as frequency increases. This qualitatively matches the trend shown by Tam[9] that the angle decreases with an increase in peak Strouhal number. It is also consistent with directionality measurements of full-scale supersonic jets and model-scale jets (see Ref. 31 Fig. 6, and Ref. 12 Fig. 11).

Figure 8 shows that at 210 Hz and at military engine conditions there exists a secondary radiation lobe. The second lobe is characterized by a directionality with a much larger polar angle. Features of the double lobe are somewhat visible in the SPLs shown in Fig. 3a, but they become much more apparent after implementation of NAH. Figures 11 and 14 of Ref. 12 also demonstrate two distinct radiation components near 210 Hz, along the reference array, for this data set. The sources of the multiple radiation components require further investigation.

The reconstructed SPLs at both 105 Hz and 210 Hz on the surfaces closest to the jet are shown in Fig. 9, projected onto the y-z plane. The region that contains levels within 3 decibels of the maximum SPL for each frequency is outlined with a black contour line. The maximum-source region of 105 Hz (shown in Fig. 9a) extends from approximately 6 m to 12 m in z. However, the maximum-source region of 210 Hz spans from about 3 m to 7 m. This shows that the source region becomes more compact and moves towards the nozzle as frequency increases.[32,33] These reconstructions support the decision to locate the center of the arc measurements downstream of the nozzle (e.g. at z = 5.5 m as explained in Sec. III),[34] although the center of the source region does vary with frequency.[12]

Note that the level distributions are not symmetric in the z direction for both frequencies shown in Fig. 9. There is a rapid drop in level in the upstream direction, but there is a more gradual drop in the downstream direction. This suggests that the estimated source distribution is asymmetric in a similar manner.[35,36]

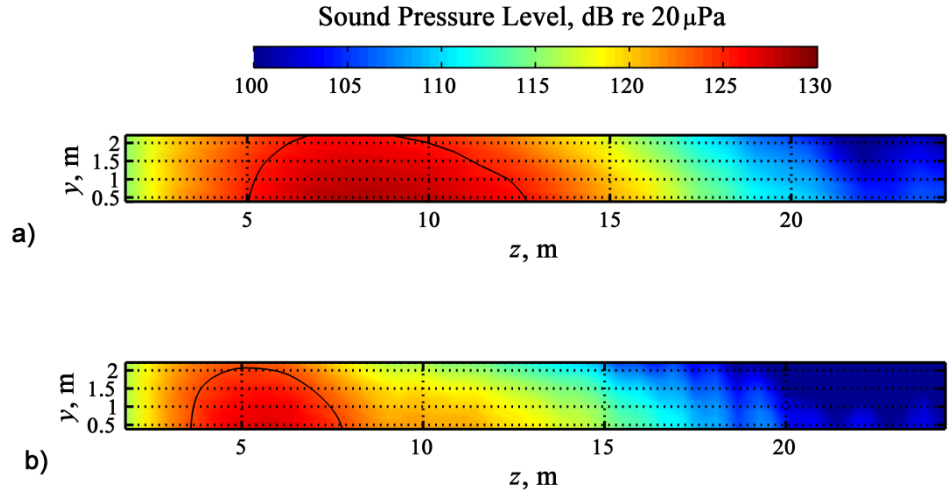

Figure 9. Reconstructed SPLs at a vertical plane, along the approximate shear layer boundary, using planar DFT-based NAH, for military power. a) 105 Hz and b) 210 Hz.

The two plane-wave NAH methods shown here likely underestimate the levels projected in toward the source. This is a result of trying to represent a geometrically spreading radiation field with plane waves; it is theoretically possible but not practical for the finite discrete measurements used in an NAH measurement, this far from the source, where much of the evanescent radiation has likely decayed below the measurement noise floor.

The results of the cylindrical DFT-based NAH implemented on the sound pressures measured by the array of reference microphones are shown in Fig. 10. Levels are plotted as a function of location, projected onto the *x*-*z* plane. The location of the reference array and the approximate shear-layer boundary are also shown. The lobe shown here is similar to the lobe shown in Fig. 5. However, the levels shown in Fig. 10 tend to grow more dramatically as the shear layer is approached than the levels shown in Fig. 5. Values inside the shear layer region serve as an equivalent source model only, since NAH projection does not account for realistic flow conditions.

To demonstrate further that the cylindrical NAH method results in a faster growth in level than the planar NAH methods as the source is approached the SPLs obtained at the shear layer boundary were calculated using both planar DFT-based NAH and cylindrical DFT-based NAH. These are shown in Fig. 11, projected onto the *z*-axis.

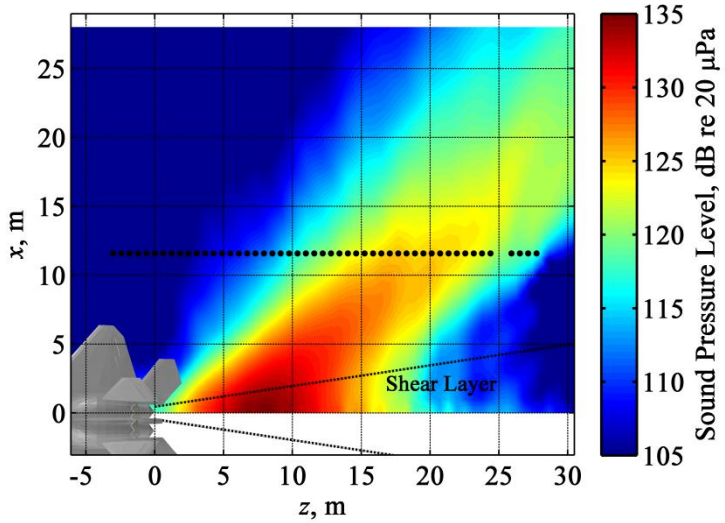

Figure 10. Cylindrical DFT-based NAH reconstruction of the sound field at 105 Hz for military power. Black dots mark the locations of the reference microphone array from which the data for the hologram were taken. The approximate location of the shear layer is also marked.

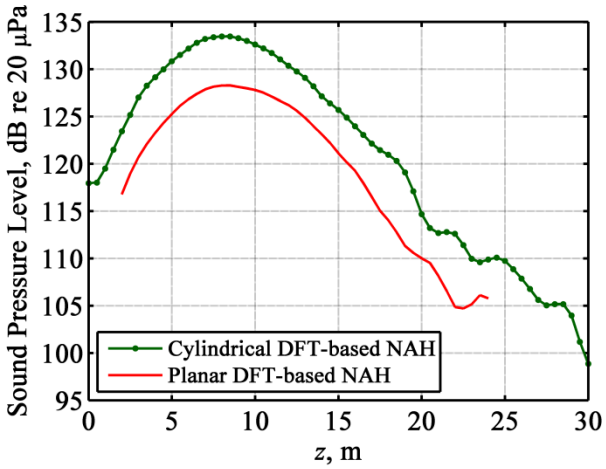

Figure 11. SPLs at 105 Hz, for military power, reconstructed at the shear layer using cylindrical DFT-based NAH and planar DFT-based NAH.

Both methods locate the maximum source region near $z = 8$, but there is a dramatic difference in the reconstructed levels—approximately 4-6 decibels at all locations.

The maximum SPL at 105 Hz, measured at plane 2, is 127.8 dB re 20 μPa, and the maximum SPL in the planar-NAH reconstruction at the shear layer is only 128.3 dB re 20 μPa, which demonstrates a 0.5 dB increase in level as the source is approached. This is probably a result of the inability of a planar representation of waves to represent accurately the geometrically spreading sound field of a localized source when important evanescent information is not captured. (Due to instrumentation limitations, such was the case for this experiment.[12]) The reconstructions shown in Figs. 10 and 11 demonstrate how a cylindrical representation of the wave field accounts for geometric spreading. Thus, cylindrical NAH methods are a promising alternative to planar NAH methods.

V. Conclusion

Sound-field reconstructions of the jet on a high-performance military aircraft were obtained from three near-field acoustical holography methods. These reconstructions show clearly the presence of strong lobing at low frequencies, which is consistent with the popular two-source model of jet noise. It was also shown that the polar angle direction characterizing this lobe decreases with increasing frequency. In addition, the source region of the jet was shown to move upstream and become more compact as frequency increases. At 210 Hz a secondary lobe that radiates at a very large polar angle was evident in the reconstruction.

The three NAH methods implemented in this experiment were planar DFT-based NAH, planar SONAH, and cylindrical DFT-based NAH. The two planar methods resulted in very similar sound-field reconstructions, so long as measurement requirements for NAH were met (i.e. dense spacing with a sufficiently large aperture). However, the planar NAH reconstructions do not reflect the properties of geometrical spreading that are expected for a jet-noise source, which is somewhat localized, particularly for an inward propagation (toward the source). This geometrical spreading is better represented when the third method, cylindrical NAH, is applied.

Acknowledgments

This research was supported in part by the appointment of A. T. Wall to the Student Research Participation Program at U.S. Air Force Research Laboratory, Human Effectiveness Directorate, Warfighter Interface Division, Battlespace Acoustics administered by the Oak Ridge Institute for Science and Education through an interagency agreement between the U.S. Department of Energy and USAFRL. Special thanks to Felicia Sexton and Hilary Gallagher for their assistance in obtaining public release of this document.

References

[1]Lee, M. and Bolton, J. S., "Source Characterization of a Subsonic Jet by Using Near-Field Acoustical Holography," *Journal of the Acoustical Society of America*, Vol. 121, No. 2, 2007, pp. 967-977.

[2]Shah, P. N., Vold, H. and Yang, M., "Reconstruction of Far-Field Noise Using Multireference Acosutical Holography Measurements of High-Speed Jets," AIAA 2011-2772, 17th AIAA/CEAS Aeroacoustics Conference, Portland, Oregon, June 5-8, 2011.

[3]Long, D., Peters, J. and Anderson, M., "Evaluating Turbofan Exhaust Noise and Source Characteristics from Near Field Measurements," AIAA 2009-3214, 15th AIAA/CEAS Aeroacoustics Conference, Miami, FL, May 2009.

[4]Wall, A. T., Gee, K. L., Gardner, M. D., Neilsen, T. B. and James, M. M., "Near-Field Acoustical Holography Applied to High-Performance Jet Aircraft Noise," *Proceedings of Meetings on Acoustics*, Vol. 9, No. 1, 2011, pp. 040009.

[5]Williams, E. G., *Fourier Acoustics: Sound Radiation and Nearfield Acoustical Holography*, Academic Press, San Diego, 1999.

[6]Wall, A. T., Gee, K. L., Neilsen, T. B., Sommerfeldt, S. D., Blotter, J. D. and James, M. M., "Statistically Optimized Near-Field Acoustical Holography Applied to a High-Power Jet," *The Journal of the Acoustical Society of America*, Vol. 129, No. 4, 2011, pp. 2492.

[7]James, M. M., Gee, K. L., Wall, A. T., Downing, J. M., Bradley, K. A. and McInerny, S. A., "Aircraft Jet Source Noise Measurements of a Lockheed Martin F-22 Fighter Jet Using a Prototype Near-Field Acoustical Holography Measurement System," *The Journal of the Acoustical Society of America*, Vol. 127, No. 3, 2010, pp. 1878.

[8]Viswanathan, K., "Mechanisms of Jet Noise Generation: Classical Theories and Recent Developments," *International Journal of Aeroacoustics*, Vol. 8, No. 4, 2009, pp. 355-408.

[9]Tam, C. K. W., Viswanathan, K., Ahuja, K. K. and Panda, J., "The Sources of Jet Noise: Experimental Evidence," *Journal of Fluid Mechanics*, Vol. 615, 2008, pp. 253-292.

[10]McInerny, S. A., Lu, G. and Olcmen, S., Report No. Under Contract UM 03-08-013, 2004.

[11]James, M. M. and Gee, K. L., "Aircraft Jet Plume Source Noise Mesurement System," *Sound and Vibration*, Vol. 44, No. 8, 2010, pp. 14-17.

[12]Wall, A. T., Gee, K. L., James, M. M., Bradley, K. A., McInerny, S. A. and Neilsen, T. B., "Near-Field Noise Measurements of a High-Performance Military Jet Aircraft," *Noise Control Engineering Journal*, submitted for publication.

[13]Lee, M. and Bolton, J. S., "Scan-Based Near-Field Acoustical Holography and Partial Field Decomposition in the Presence of Noise and Source Level Variation," *Journal of the Acoustical Society of America*, Vol. 119, No. 1, 2006, pp. 382-393.

[14]Williams, E. G. and Maynard, J. D., "Holographic Imaging without the Wavelength Resolution Limit," *Physical Review Letters*, Vol. 45, No. 7, 1980, pp. 554-557.

[15]Wang, Z. and Wu, S. F., "Helmholtz Equation--Least-Squares Method for Reconstructing the Acoustic Pressure Field," *The Journal of the Acoustical Society of America*, Vol. 102, No. 4, 1997, pp. 2020-2032.

[16]Williams, E. G., "Regularization Methods for Near-Field Acoustical Holography," *Journal of the Acoustical Society of America*, Vol. 110, No. 4, 2001, pp. 1976-1988.

[17]Williams, E. G., "Continuation of Acoustic Near-Fields," *Journal of the Acoustical Society of America*, Vol. 113, No. 3, 2003, pp. 1273.

[18]Scholte, R., Lopez, I., Roozen, N. B. and Nijmeijer, H., "Truncated Aperture Extrapolation for Fourier-Based Near-Field Acoustic Holography by Means of Border-Padding," *Journal of the Acoustical Society of America*, Vol. 125, No. 6, 2009, pp. 3844-3854.

[19]Yang, C., Chen, J., Xue, W.-F. and Li, J.-q., "Progress of the Patch Near-Field Acoustical Holography Technique," *Acta Acustica united with Acustica*, Vol. 94, No. 1, 2008, pp. 156-163.

[20]Hald, J., "Basic Theory and Properties of Statistically Optimized Near-Field Acoustical Holography," *Journal of the Acoustical Society of America*, Vol. 125, No. 4, 2009, pp. 2105-2120.

[21]Hallman, D. L. and Bolton, J. S., "A Comparision of Multi-Reference Nearfield Acoustical Holography Procedures," Proceedings of NOISE-CON 94, Ft. Lauderdale, Florida, 1994, pp. 929-933.

[22]Price, S. M. and Bernhard, R. J., "Virtual Coherence: A Digital Signal Processing Technique for Incoherent Source Idientification," *Proceedings of 4th International Modal Analysis Conference*, Los Angleles, CA, 1986, pp. 1256-1262.

[23]Maynard, J. D., Williams, E. G. and Lee, Y., "Nearfield Acoustic Holography: 1. Theory of Generalized Holography and the Development of NAH," *Journal of the Acoustical Society of America*, Vol. 78, No. 4, 1985, pp. 1395-1413.

[24]Pierce, A. D., *Acoustics: An Introduction to Its Physical Principles and Applications*, 1994 ed., Acoustical Society of America, Melville, NY, 1989, pp. 208-210.

[25]Wall, A. T., Gee, K. L., Krueger, D. W., Neilsen, T. B. and Sommerfeldt, S. D., "Aperture Extension for Near-Field Acoustical Holography of Jet Noise," *Proceedings of Meetings on Acoustics*, Vol. 14, unpublished.

[26]Krueger, D. W., *Array-Based Characterization of Military Jet Aircraft Noise* (M.S. Thesis, Brigham Young University, Provo, to be submitted 2012).

[27]Cho, Y. T., Bolton, J. S. and Hald, J., "Source Visualization by Using Statistically Optimized Near-Field Acoustical Holography in Cylindrical Coordinates," *Journal of the Acoustical Society of America*, Vol. 118, No. 4, 2005, pp. 2355.

[28]Ginn, K. B. and Hald, J., "STSF-Practical Instrumentation and Applications," *Bruel & Kjaer Tecnical Review*, No. 2, 1989, pp. 1-27.

[29]J. Hald, "STSF—A unique technique for scan-based nearfield acoustical holography without restriction on coherence," Technical Report No. 1, from Bruel & Kjaer, Naerum, Denmark, 1989.

[30]Tam, C. K. W., Viswanathan, K., Pastouchenko, N. N. and Tam, B., "Continuation of the Near Acoustic Field of a Jet to the Far Field. Part II: Experimental Validation and Noise Source Characteristics," AIAA 2010-3729, 16th AIAA/CEAS Aeroacoustics Conference, Stockholm, Sweeden, June 7-9, 2010.

[31]Schlinker, R. H., Liljenberg, S. A., Polak, D. R., Post, K. A., Chipman, C. T. and Stern, A. M., "Supersonic Jet Noise Source Characteristics & Propagation: Engine and Model Scale," AIAA 2007-3623, 13th AIAA/CEAS Aeroacsoustics Conference, Rome, Italy, May 21-23, 2007.

[32]Lee, S. S. and Bridges, J., "Phased-Array Measurements of Single Flow Hot Jets," AIAA 2005-2842, 11th AIAA/CEAS Aeroacoustics Conference, Monterey, CA, May 2005.

[33]Papamoschou, D., "Imaging of Directional Distributed Noise Sources," AIAA 2008-2885, 14th AIAA/CEAS Aeroacoustics Conference, Vancouver, British Columbia, Candada, May 2008.

[34]Gee, K. L., et al., "The Role of Nonlinear Effects in the Propagation of Noise from High-Power Jet Aircraft," *The Journal of the Acoustical Society of America*, Vol. 123, No. 6, 2008, pp. 4082-4093.

[35]Schlinker, R. H., *Supersonic Jet Noise Experiments* (Ph.D. Dissertation, University of Southern California, Los Angeles, CA, 1975).

[36]Tam, C. K. W., Pastouchenko, N. N. and Schlinker, R. H., "Noise Source Distribution in Supersonic Jets," *Journal of Sound and Vibration*, Vol. 291, No. 1-2, 2006, pp. 192-201.